

Optimized blue-phase liquid crystal for field-sequential-color displays

YUGE HUANG,¹ HAIWEI CHEN,¹ GUANJUN TAN,¹ HITOSHI TOBATA,² SHIN-ICHI YAMAMOTO,² EIJI OKABE,² YI-FEN LAN,³ CHENG-YEH TSAI,³ AND SHIN-TSON WU^{1,*}

¹College of Optics and Photonics, University of Central Florida, Orlando, FL 32816, USA

²JNC Petrochemical Corporation, Ichihara Research Center, Ichihara, Chiba 290-8551, Japan

³Advanced Display Technology Centre, AU Optronics Corp., Hsinchu 30078, Taiwan

*swu@ucf.edu

Abstract: We report an optimized blue phase liquid crystal (BPLC) mixture JC-BP08 for field-sequential-color (FSC) display applications. JC-BP08 exhibits several attractive features: 1) its fast average gray-to-gray response time enables FSC display, which in turn triples the resolution density and optical efficiency. 2) Its voltage holding ratio is >99.4% at 25°C and >93.2% at 60°C. 3) Its average dielectric constant $\epsilon' \approx 87$ is still manageable by the bootstrapping driving to enable 240 Hz operation. 4) Using a triangular protrusion electrode structure, the transmittance can reach 74% at 15V, which enables single-TFT driving. 5) With two-domain structure, it offers indistinguishable gamma shift and wide viewing angle. We proposed voltage charging model and found a linear relationship between the required charging time and ϵ' , which is validated by our experimental results.

© 2017 Optical Society of America

OCIS codes: (160.3710) Liquid crystals; (120.2040) Displays.

References and links

1. H. Kikuchi, M. Yokota, Y. Hisakado, H. Yang, and T. Kajiyama, "Polymer-stabilized liquid crystal blue phases," *Nat. Mater.* **1**(1), 64–68 (2002).
2. J. Yan, L. Rao, M. Jiao, Y. Li, H. C. Cheng, and S. T. Wu, "Polymer-stabilized optically isotropic liquid crystals for next-generation display and photonics applications," *J. Mater. Chem. C Mater. Opt. Electron. Devices* **21**, 7870–7877 (2011).
3. Z. Ge, L. Rao, S. Gauza, and S. T. Wu, "Modeling of blue phase liquid crystal displays," *J. Disp. Technol.* **5**(7), 250–256 (2009).
4. H. Lee, H. J. Park, O. J. Kwon, S. J. Yun, J. H. Park, S. Hong, and S. T. Shin, "The world's first blue phase liquid crystal display," *SID Int. Symp. Dig. Tech. Pap.* **42**(1), 121–124 (2011).
5. C. Y. Tsai, F. C. Yu, Y. F. Lan, P. J. Huang, S. Y. Lin, Y. T. Chen, T. I. Tsao, C. T. Hsieh, B. S. Tseng, C. W. Kuo, C. H. Lin, C. C. Kuo, C. H. Chen, H. Y. Hsieh, C. T. Chuang, N. Sugiura, C. L. Lin, and M. H. Cheng, "A novel blue phase liquid crystal display applying wall-electrode and high driving voltage circuit," *SID Int. Symp. Dig. Tech. Pap.* **46**(1), 542–544 (2015).
6. L. Rao, Z. Ge, S. T. Wu, and S. H. Lee, "Low voltage blue-phase liquid crystal displays," *Appl. Phys. Lett.* **95**(23), 231101 (2009).
7. M. Kim, M. S. Kim, B. G. Kang, M. K. Kim, S. Yoon, S. H. Lee, Z. Ge, L. Rao, S. Gauza, and S. T. Wu, "Wall-shaped electrodes for reducing the operation voltage of polymer-stabilized blue phase liquid crystal displays," *J. Phys. D: Appl. Phys.* **42**(23), 235502 (2009).
8. L. Rao, J. Yan, S. T. Wu, S. Yamamoto, and Y. Haseba, "A large Kerr constant polymer-stabilized blue phase liquid crystal," *Appl. Phys. Lett.* **98**(8), 081109 (2011).
9. Y. Chen, D. Xu, S. T. Wu, S. Yamamoto, and Y. Haseba, "A low voltage and submillisecond-response polymer-stabilized blue phase liquid crystal," *Appl. Phys. Lett.* **102**(14), 141116 (2013).
10. F. Peng, Y. Chen, J. Yuan, H. Chen, S. T. Wu, and Y. Haseba, "Low temperature and high frequency effects on polymer-stabilized blue phase liquid crystals with large dielectric anisotropy," *J. Mater. Chem. C Mater. Opt. Electron. Devices* **2**(18), 3597–3601 (2014).
11. M. Wittek, N. Tanaka, D. Wilkes, M. Bremer, D. Pauluth, J. Canisius, A. Yeh, R. Yan, K. Skjonnemand, and M. Klasen-Memmer, "New materials for polymer-stabilized blue phase," *SID Int. Symp. Dig. Tech. Pap.* **43**(1), 25–28 (2012).
12. Y. Haseba, S. I. Yamamoto, K. Sago, A. Takata, and H. Tobata, "Low-voltage polymer-stabilized blue-phase liquid crystals," *SID Int. Symp. Dig. Tech. Pap.* **43**(1), 254–257 (2013).

13. C. D. Tu, C. L. Lin, J. Yan, Y. Chen, P. O. Lai, and S. T. Wu, "Driving scheme using bootstrapping method for blue-phase LCDs," *J. Disp. Technol.* **9**(1), 3–6 (2013).
14. C. L. Lin, C. D. Tu, M. H. Cheng, C. C. Hung, C. H. Lin, and N. Sugiura, "Novel dual-coupling pixel circuit to achieve high transmittance of blue-phase liquid crystal," *IEEE Electron Device Lett.* **36**(4), 354–356 (2015).
15. F. C. Lin, Y. P. Huang, and H. P. D. Shieh, "Color breakup reduction by 180 Hz stencil-FSC method in large-sized color filter-less LCDs," *J. Disp. Technol.* **6**(3), 107–112 (2010).
16. Y. Li, Y. Chen, J. Sun, S. T. Wu, S. H. Liu, P. J. Hsieh, K. L. Cheng, and J. W. Shiu, "Dielectric dispersion on the Kerr constant of blue phase liquid crystals," *Appl. Phys. Lett.* **99**(18), 181126 (2011).
17. Y. Chen and S. T. Wu, "Recent advances on polymer-stabilized blue phase liquid crystal materials and devices," *J. Appl. Polym. Sci.* **131**(13), 40556 (2014).
18. P. C. Wu, H. T. Hsu, H. L. Chen, and W. Lee, "Dielectric characterization and voltage holding ratio of blue-phase cells," *Displays* **44**, 66–72 (2016).
19. J. Yan, H. C. Cheng, S. Gauza, Y. Li, M. Jiao, L. Rao, and S. T. Wu, "Extended Kerr effect of polymer-stabilized blue-phase liquid crystals," *Appl. Phys. Lett.* **96**(7), 071105 (2010).
20. P. R. Gerber, "Electro-optical effects of a small-pitch blue-phase system," *Mol. Cryst. Liq. Cryst. (Phila. Pa.)* **116**(3–4), 197–206 (1985).
21. Y. P. Huang, F. C. Lin, and H. P. D. Shieh, "Eco-displays: the color LCD's without color filters and polarizers," *J. Disp. Technol.* **7**(12), 630–632 (2011).
22. H. C. Cheng, L. Rao, and S. T. Wu, "Color breakup suppression in field-sequential five-primary-color LCDs," *J. Disp. Technol.* **6**(6), 229–234 (2010).
23. S. T. Wu, "Birefringence dispersions of liquid crystals," *Phys. Rev. A Gen. Phys.* **33**(2), 1270–1274 (1986).
24. M. Hird, "Fluorinated liquid crystals-properties and applications," *Chem. Soc. Rev.* **36**(12), 2070–2095 (2007).
25. T. Ishitani, Y. Niikura, M. Ikenaga, M. Kobayashi, M. Kato, Y. Oe, M. Nakano, H. Shishido, Y. Hirakata, S. Yamazaki, and D. Kurosaki, "High-performance polymer-stabilized blue-phase LCD with low driving voltage," *J. Soc. Inf. Disp.* **21**(1), 9–15 (2013).
26. S. Yoon, M. Kim, M. S. Kim, B. G. Kang, M. K. Kim, A. K. Srivastava, S. H. Lee, Z. Ge, L. Rao, S. Gauza, and S. T. Wu, "Optimisation of electrode structure to improve the electro-optic characteristics of liquid crystal display based on Kerr effect," *Liq. Cryst.* **37**(2), 201–208 (2010).
27. Y. Li, S. Huang, N. Rong, J. G. Lu, C. P. Chen, X. Li, P. Zhou, Y. Yuan, S. Liu, G. He, and Y. Su, "Transmissive and transfective blue-phase LCDs with double-layer IPS electrodes," *J. Disp. Technol.* **12**(2), 122–128 (2016).
28. J. Liu, H. Ma, and Y. Sun, "Blue-phase liquid crystal display with high dielectric material," *Liq. Cryst.* **43**(12), 1748–1752 (2016).
29. T. Yamamoto, M. Ikenaga, A. Yamashita, D. Kubota, M. Nakano, T. Ishitani, H. Shishido, Y. Hirakata, S. Yamazaki, R. Sato, K. Okazaki, M. Katayama, and T. Akahane, "Crystalline OS-LCD using blue-phase liquid crystal having characteristic texture," *SID Int. Symp. Dig. Tech. Pap.* **43**(1), 201–204 (2012).
30. D. Kubota, A. Yamashita, and M. Nakano, "Liquid crystal display device," United States Patent No. 8,786,811 B2 (Jul. 22, 2014).
31. H. Chen, Y. F. Lan, C. Y. Tsai, and S. T. Wu, "Low-voltage blue-phase liquid crystal display with diamond-shape electrodes," *Liq. Cryst.*, doi:10.1080/02678292.2016.1264014.
32. L. Rao, Z. Ge, and S. T. Wu, "Zigzag electrodes for suppressing the color shift of Kerr effect-based liquid crystal displays," *J. Disp. Technol.* **6**(4), 115–120 (2010).
33. S. S. Kim, B. H. Berkeley, K. H. Kim, and J. K. Song, "New technologies for advanced LCD-TV performance," *J. Soc. Inf. Disp.* **12**(4), 353–359 (2004).
34. Y. Gao, Z. Luo, R. Zhu, Q. Hong, S. T. Wu, M. C. Li, S. L. Lee, and W. C. Tsai, "A high performance single-domain LCD with wide luminance distribution," *J. Disp. Technol.* **11**(4), 315–324 (2015).

1. Introduction

Polymer-stabilized blue phase liquid crystal (PS-BPLC) [1,2] exhibits several attractive features for display and photonic applications, such as submillisecond response time, no need for surface alignment, optically isotropic dark state, and insensitive to the cell gap if an in-plane switching (IPS) cell is employed [3]. However, after ~15 years of extensive efforts, BPLC still remains at the prototype stage [4,5]. The major hurdles are twofold: 1) high operation voltage (V_p) and 2) slow capacitor charging for active matrix addressing. High V_p dramatically increases the power consumption, while slow charging limits the device resolution and frame rate. To reduce V_p , two main approaches have been commonly practiced: protruded electrodes [6,7] and large Kerr constant BPLC materials [8–10]. To enhance Kerr constant, several BPLC materials with $\Delta n > 0.18$ and $\Delta \epsilon > 100$ have been developed [11,12]. The major concerns for such a huge $\Delta \epsilon$ BPLC material are: 1) increased rotational viscosity (γ_1), which leads to a slower response time (> 1 ms), and 2) longer capacitor charging time when addressed by TFTs (thin film transistors); this problem

magnifies as display resolution or frame rate increases. To overcome the slow charging issue, bootstrapping driving, i.e. pre-charging method has been developed [13,14]. If the average dielectric constant (ϵ') is smaller than 100, then the charging issue can still be managed. But the dilemma stays: lower $\Delta\epsilon$ leads to increased V_p . Therefore, a delicate balance between operation voltage, response time, and charging time has to be taken into consideration. An ideal BPLC should possess following properties: fast charging time for high resolution and high frame rate, high transmittance at 15 V for single-TFT driving, and submillisecond response time for field-sequential-color (FSC) displays [15]. FSC eliminates the need of color filters so that it triples the optical efficiency and resolution density. These features are highly desirable for the emerging wearable virtual reality and augmented reality display applications.

In this paper, we report a BPLC mixture, called JC-BP08, which is optimized for FSC displays. Its physical properties are listed as follows: $\epsilon' \approx 87$ so that the TFT charging issue is still manageable, VHR >99.4% at 25°C once charged, and response time 0.83 ms at room temperature (RT). Using a protruded electrode structure, our simulation results indicate that we can obtain transmittance ~74% at 15 V using JC-BP08. This is an important step towards single TFT (per pixel) addressing.

2. Experimental results and discussion

2.1 Materials and measurement

In the past few years, three commercial BPLC mixtures have been well studied; they are PSBP-01 (JNC, Japan) [8,12,16], Merck BPLC [11], and HTG-135200 (HCCH, China) [17,18]. Among them, Merck's mixture is only available to some specific customers. JNC's PSBP-01 has a relatively large Kerr constant, which helps to lower the operation voltage. However, its decay time is around 1.6 ms, which is fast for conventional 120-Hz framerate operation, but not fast enough for FSC, which demands ≥ 240 Hz in order to mitigate color breakup. Finally, the HCCH's mixture is for experimental studies only, not intended for active matrix display applications because of its relatively low voltage holding ratio (VHR \approx 80%) [18].

Here, we prepared a new BPLC mixture: JC-BP08 (from JNC). The compositions and UV curing conditions are described as follows: JC-BP08 precursor contains 84 wt. % nematic LC host, 4.8% chiral dopant, 10.8% monomers, and 0.4% photoinitiator. The dielectric anisotropy and birefringence of the LC host of JC-BP08 are $\Delta\epsilon = 114$ (at $f = 1$ kHz and 25°C) and $\Delta n = 0.161$ ($\lambda = 589$ nm and 25°C), respectively. Before UV curing, the phase transition temperatures are: N* 53.0°C BP during heating and BP 50.8°C N* during cooling, where N* stands for chiral nematic phase. After UV curing at BP-I, the physical properties of polymer-stabilized JC-BP08 are: $\epsilon' = 87$ at $f = 60$ Hz and 25°C, clearing temperature $T_C = 75^\circ\text{C}$, and melting point $T_{mp} < -20^\circ\text{C}$.

To characterize the electro-optic performance, we filled JC-BP08 into an IPS cell with no surface alignment layer. Because JC-BP01 has a similar ϵ' value, we include it as benchmark for comparison. The IPS-8/12 cells we employed have ITO electrode width $w = 8$ μm , electrode gap $g = 12$ μm , and cell gap $d = 7.3$ μm . When heated to BP-I, the cells were cured under UV light ($\lambda \sim 365$ nm, intensity 8 mW/cm²) for 15 min. For convenience, we call the two samples as PSBP-01 and PSBP-08. Our experiment was conducted at RT unless otherwise mentioned.

Figures 1(a) and 1(b) depict the measured voltage-dependent transmittance (VT) curves and temperature dependent decay time of PSBP-01 and PSBP-08, respectively. Here, the transmittance is normalized to that of two parallel polarizers. We also fit the experimental VT curves with the extended Kerr effect model, in which the induced birefringence Δn_{ind} is related to the electric field E as [19]:

$$\Delta n_{ind} = \Delta n_s \left(1 - \exp \left[- \left(E / E_s \right)^2 \right] \right), \quad (1)$$

where Δn_s stands for the saturated birefringence and E_s for the saturation electric field. As Fig. 1(a) depicts, Eq. (1) fits the measured VT curves of PSBP-01 and PSBP-08 well by TechWiz (SANAYI System). Through fittings, we found $\Delta n_s = 0.138$ and $E_s = 6.0 \text{ V}/\mu\text{m}$ for PSBP-08, and $\Delta n_s = 0.135$ and $E_s = 4.7 \text{ V}/\mu\text{m}$ for PSBP-01. Based on these parameters, we obtained Kerr constant $K = 6.1 \text{ nm}/\text{V}^2$ for PSBP-08, and $K = 9.7 \text{ nm}/\text{V}^2$ for PSBP-01. Our Kerr constant of PSBP-01 is somewhat smaller than that reported in [8], because our measurement is at a higher temperature. As Figs. 1(a) and 1(b) depict, PSBP-01 shows a lower V_p than PSBP-08 because of its larger Kerr constant, but its response time is $>2x$ slower than that of PSBP-08 at RT. This difference amplifies in the low temperature region. The difference between PSBP-01 and PSBP-08 mainly comes from the average elastic constant k , which contributes to Kerr constant K and response time τ by the following equations [2,20]:

$$K \approx \frac{\Delta n \Delta \epsilon P^2}{k \lambda (2\pi)^2}, \quad (2)$$

$$\tau \approx \frac{\gamma_1 P^2}{k (2\pi)^2}, \quad (3)$$

where Δn , $\Delta \epsilon$, P , and γ_1 represent the birefringence, dielectric anisotropy, pitch length, and rotational viscosity of the BPLC composite, respectively, and λ is the wavelength. JC-BP01 has its advantage of large Kerr constant, so the low operation voltage makes it useful for general displays. However, submillisecond response time is essential for FSC displays in order to suppress color breakup [21,22]. To achieve a faster response time than JC-BP01, our JC-BP08 exhibits a larger k , which helps to shorten the response time (Eq. (3)) but its Kerr constant is somewhat compromised (Eq. (2)). The pitch length is also slightly adjusted from $P = 412 \text{ nm}$ for PSBP-01 to $P = 376 \text{ nm}$ for PSBP-08.

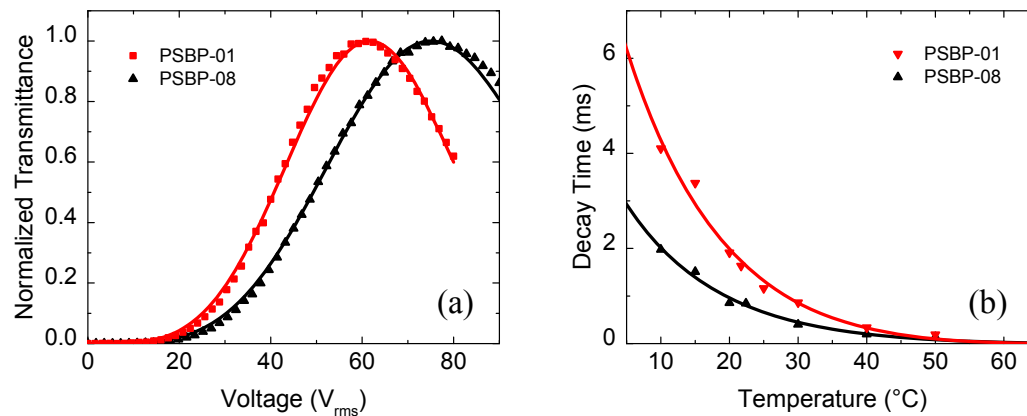


Fig. 1. (a) VT curves at RT and (b) temperature-dependent decay time of PSBP-01 and PSBP-08 at $\lambda = 633 \text{ nm}$ and frame rate = 240 Hz. Dots are experimental data and lines are fitting curves.

PSBP-08 is particularly attractive for FSC displays because of its sub-millisecond response time. Table 1 lists the measured gray-to-gray (GTG) response time (τ) of PSBP-08 at RT *without* overdrive and undershoot voltages. The averaged GTG rise time is 0.9 ms and decay time is 1.0 ms.

Table 1. Measured response time of PSBP-08 between different grey levels (1-8)

		Rise time (ms)							
Decay time (ms)		1	2	3	4	5	6	7	8
	1		1.827	1.775	1.490	1.476	1.330	1.129	0.560
	2	0.258		1.028	1.197	1.096	1.035	0.862	0.326
	3	0.317	0.879		0.935	1.024	1.202	0.988	0.357
	4	0.351	0.831	0.602		0.868	0.821	0.749	0.350
	5	0.415	0.798	1.103	1.393		0.723	0.683	0.324
	6	0.445	0.884	0.959	1.245	1.607		0.632	0.292
	7	0.546	1.003	1.124	1.274	1.231	1.183		0.246
	8	0.846	1.525	1.393	1.330	1.413	1.359	1.482	

2.2 Wavelength and frequency effects of PSBP-08

For a given PSBP composite, Δn_s governs its optical response, e.g. transmittance, while E_s determines its operation voltage. Both Δn_s and E_s influence Kerr constant by [16]

$$K = \Delta n_s / (\lambda E_s^2). \quad (4)$$

Equation (4) implies that to lower the operating voltage (i.e. larger Kerr constant), higher Δn_s , shorter wavelength and lower E_s are preferred.

2.2.1 Wavelength effect

Figure 2 depicts the wavelength effect of PSBP-08. In Fig. 2(a), we fixed $E_s = 6.0 \text{ V}/\mu\text{m}$ at $f = 240 \text{ Hz}$ and fitted the VT curves at the specified wavelengths. The obtained Δn_s values are plotted in Fig. 2(b). We further fitted the Δn_s dispersion with following equation [23]:

$$\Delta n_s = G \frac{\lambda^2 \lambda^{*2}}{\lambda^2 - \lambda^{*2}}, \quad (5)$$

and obtained the proportionality constant $G = 2.07 \mu\text{m}^{-2}$ and the mean resonance wavelength $\lambda^* = 239 \text{ nm}$. From Eq. (5), we find $\Delta n_s = 0.146$ at $\lambda = 550 \text{ nm}$ for PSBP-08.

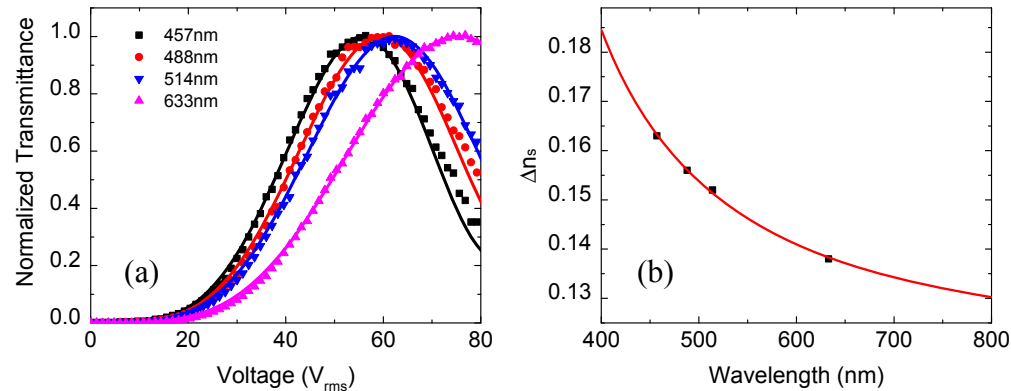


Fig. 2. (a) Measured and fitted VT curves of PSBP-08 at the specified wavelengths, 240 frame/second and RT. Dots are measured data; lines are fitting curves with Eq. (1) by fixing $E_s = 6.0 \text{ V}/\mu\text{m}$. (b) Dispersion of Δn_s for PSBP-08. Dots are results obtained from (a) and red line represents the fitting with Eq. (5).

2.2.2 Frequency effect

A higher TFT frame rate helps to mitigate color breakup, but the tradeoff is increased electronic power consumption. To balance these two effects, most LCD TVs are operated at 120 frames per second (frequency $f = 60 \text{ Hz}$). For FSC displays, in order to reduce color

breakup, the frame rate should be 240 Hz ($f = 120$ Hz) or higher. Figure 3(a) depicts the frequency dependent VT curves. As the frequency increases from 60 Hz to 2 kHz, V_p increases gradually. To fit each VT curve, we fixed $\Delta n_s = 0.138$ (for $\lambda = 633$ nm) and obtained different E_s values. Based on the Δn_s and E_s values, we calculated the Kerr constant as plotted in Fig. 3(b). Next, we fitted the experimental data with following extended Cole-Cole equation [16]:

$$K(f) = K_\infty + (K_s - K_\infty) \frac{1 + \left(\frac{f}{f_r}\right)^{1-\alpha} \sin \frac{1}{2} \alpha \pi}{1 + 2 \left(\frac{f}{f_r}\right)^{1-\alpha} \sin \frac{1}{2} \alpha \pi + \left(\frac{f}{f_r}\right)^{2(1-\alpha)}}. \quad (6)$$

Through fittings, we find the static Kerr constant $K_s = 6.5$ nm/V², high frequency Kerr constant $K_\infty = 0$, Debye relaxation frequency $f_r = 1.2$ kHz, and $\alpha = 0.13$. For comparison, $f_r = 1.3$ kHz for PSBP-01 [16]. Since PSBP-08 has a similar ϵ' to PSBP-01, their f_r values are also comparable. As Fig. 3(b) depicts, Kerr constant decreases gradually as the frequency increases. At $f = 120$ Hz (frame rate 240 Hz), the Kerr constant slightly decreases to 6.1 nm/V².

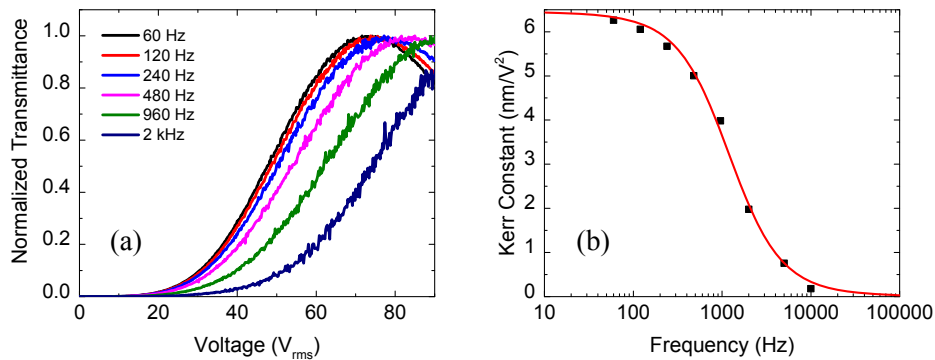


Fig. 3. (a) Measured frequency-dependent VT curves of PSBP-08 at $\lambda = 633$ nm and RT. (b) Frequency dependent Kerr constant of PSBP-08. Black dots are the extracted data from (a), while red line represents fitting with Eq. (6).

2.3 Charging issue for high dielectric constant BPLC materials

Fast capacitor charging time plays a key role for FSC and high-resolution display devices. In 2013, Haseba, et al. [12] used PSBP-06 to demonstrate that LC with a larger dielectric constant (ϵ') needs a longer time to be fully charged. A higher ϵ' LC implies to a larger capacitor, as a result, it requires a longer time to accumulate the electric charges. Similar to Kerr constant, the dielectric constant of BPLC declines as the driving frequency increases. A short (typically 20 μ s) DC voltage from TFT contains some high frequency components. From Fig. 3(b), during such a short charging time, the corresponding ϵ' value is very small. Since the following frame time is much longer than the charging time, the voltage-holding frequency is much lower than the charging frequency. At the beginning of open circuit, the working frequency drops quickly from the high charging frequency to the low voltage-holding frequency, thus ϵ' and the capacitance increase instantly, resulting in a low charged-in voltage. Nematic LCs do not suffer such problem because their ϵ' is small and ϵ' is insensitive to the driving frequency as long as $f < 100$ kHz.

To illustrate the slow charging time and low VHR issues of a BP LCD, let us assume the applied voltage is $V_o = 10$ V and charging time $t_c = 16$ μ s. Because the BPLC has a large

capacitance, it requires much longer time to reach 10V. With such a short charging time, the charged-in voltage V_i is about 4.2 V, which is much lower than V_o , as Fig. 4(a) shows. After a holding time of $t_h = 8.3$ ms [240 frame/second], the held voltage decreases to V_h . Therefore, two parameters determine the electrical performance of a BP LCD: 1) charging time: it is related to ϵ' and f_r , which indicates how ϵ' changes with frequency; 2) VHR defined as V_h/V_i : it represents how well the voltage is held in a given frame time. Our PSBP-08 has a moderate ϵ' , its charging time is about 250 μ s, which is still more than 10x longer than that of a conventional nematic LC. But once charged, its VHR reaches 99.4% at 25°C and 93.2% at 60°C. The high VHR is because JC-BP08 consists of mainly fluorinated multi-ring compounds [17]. Fluorinated LCs exhibit a high resistivity, which leads to a large VHR [24], and have been widely used in TFT LCDs.

In principle, we should compare the charging issues of our PSBP-08 with PSBP-01 directly. However, there are no such data available for PSBP-01. Instead, we found the experimental data of PSBP-06 reported in [12]. Figure 4(b) shows the measured V_i/V_o of PSBP-06 (red dots) and our measured PSBP-08 (black triangles). PSBP-06 has a very large ϵ' (~ 200), so its required charging time is about 1.5 ms. To understand the slow charging phenomenon, we propose following equations:

$$V_i/V_o = 1 - \exp(-t_c/t_0), \quad (7)$$

$$t_0 = b \cdot \epsilon'(f), \quad (8)$$

$$f = \frac{1}{2t_c}, \quad (9)$$

where t_c is the charging time (a variable), t_0 is a characteristic charging time, which is linearly proportional to ϵ' by a constant b , and f is the driving frequency ($= 0.5 \times$ frame rate). First, we fit the red dots in Fig. 4(b) with Eqs. (7)-(9), as the red line shows, and obtain $b = 1.704$. The agreement between model and experiment is very good. Next, we use the same b value to fit our PSBP-08 data *without* any adjustable parameter. Results are shown by the black line. Again, the agreement is good, although we have only two data points. Therefore, our model is validated experimentally. As shown in Fig. 4(b), PSBP-06 has a huge ϵ' , which is desirable for lowering the operation voltage, but the required charging time is 1.5 ms. By contrast, PSBP-08 has a smaller ϵ' so that its required charging time (~ 250 μ s) is shortened by 6x, which is easier to be addressed by the pre-charging method [13,14].

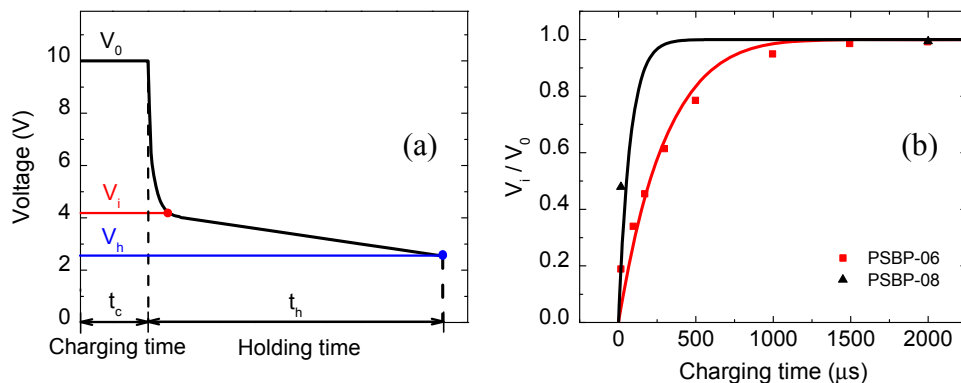


Fig. 4. (a) Schematic illustration of the charged-in voltage and voltage holding ratio. t_c , t_h , V_o , V_i and V_h stand for charging time, holding time, applied voltage, charged-in voltage and held voltage, respectively. (b) Charging time dependent V_i/V_o , where dots are experimental data and lines are fitting curves according to Eqs. (7)-(9).

3. Device simulation

Although we have overcome the charging issues, the high driving voltage is PSBP-08's Achilles heel. Our target is to lower the operation voltage to 15V to enable single-TFT addressing, while keeping a reasonably high transmittance, say >70%. In this Section, we perform device simulation using PSBP-08 in some reported protrusion structures.

3.1 Protrusion electrode for low driving voltage

In 2009, Rao, et al. [6] proposed a protruded electrode structure for lowering the operation voltage. This approach is proven to be quite effective. Several groups have fabricated such structures [4,5,25], especially in 2015 AUO demonstrated such protrusion electrodes in a 10⁷ BPLC prototype [5]. The peak transmittance is over 75%, but the operation voltage is 32 V so that two TFTs per pixel are required. High V_p increases the power consumption while two TFTs reduce the aperture ratio and optical efficiency.

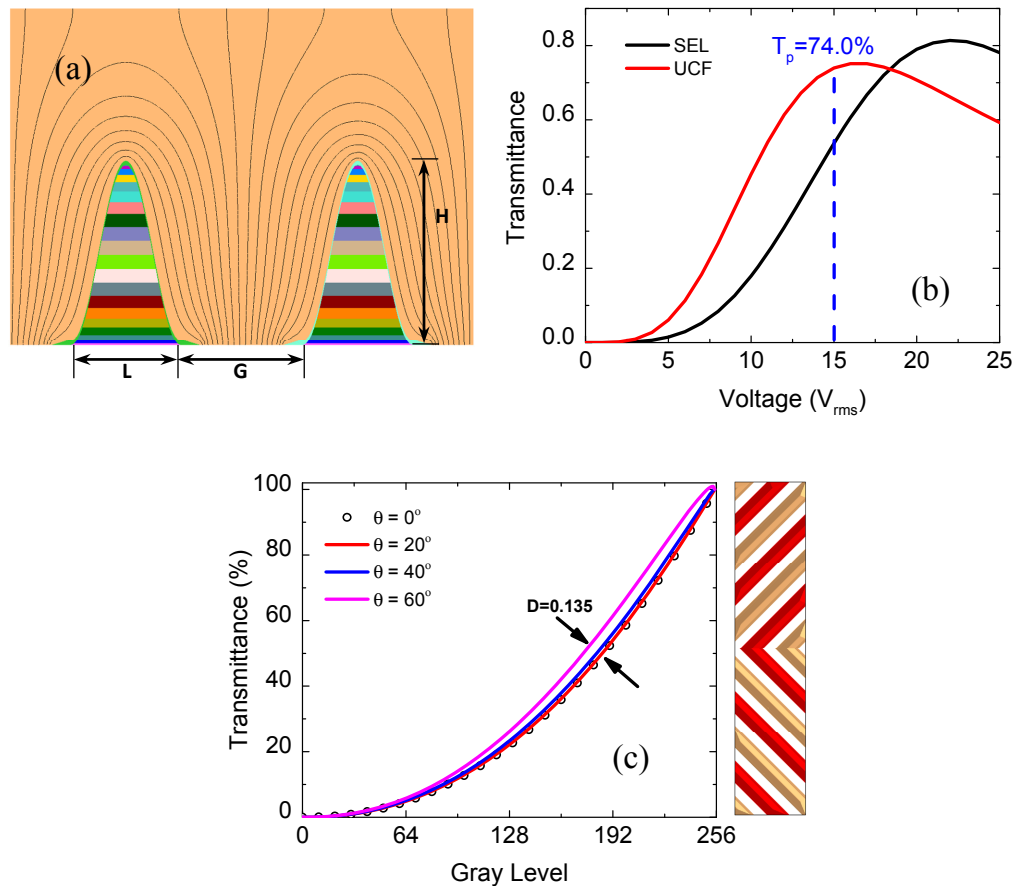


Fig. 5. (a) The triangular electrode structure used in simulation, where $H = 2.14 \mu\text{m}$, $L = 1.32 \mu\text{m}$, cell gap $d = 4 \mu\text{m}$, and the ITO tails beside the protrusion are kept for applying voltage. (b) Simulated VT curves of PSBP-08 ($\lambda = 550 \text{ nm}$, 240 frame/second) using the triangular electrode structure. The black and red lines refer to using the original protrusion gap $G = 2.68 \mu\text{m}$ and using our optimized protrusion gap $G = 1.5 \mu\text{m}$, respectively. (c) Viewing angle dependence of gamma curves for film-compensated two-domain triangular electrode structure along the most severe gamma shift direction ($\varphi = 230^\circ$). The right picture shows the two-domain structure configuration. Red and orange denote common and pixel electrodes, respectively.

For the protrusion structure, fabrication technique limits the best performance that can be achieved. As Fig. 5(a) depicts, to lower V_p , we could decrease the protrusion gap G to increase the electric field intensity between two protrusions, or increase protrusion height H for the incoming light to accumulate more phase retardation. Nevertheless, narrower G demands a smaller protrusion width L to keep high transmittance, since the area above the protrusion is a dead zone. Under such a condition, tall and thin protrusion is favored, but of course, they are more challenging to fabricate. Several other electrode structures have been proposed, but the fabrication is a limiting factor in practice [26–28]. In 2012, Yamamoto, et al. proposed and fabricated a triangular electrode structure (Fig. 5(a)) to improve contrast ratio [29,30], whose protrusion height is $H = 2.14\mu\text{m}$ and length $L = 1.32\mu\text{m}$. A diamond-shape electrode structure is also proposed, which exhibits a promising performance [31].

3.2 Performance of PSBP-08 on protruded electrodes

Here, we study the performance of our PSBP-08 using the protruded triangular electrodes. In Fig. 5(a), a ridge protrusion is deposited on the bottom substrate, then ITO stripes are sputtered onto the ridge protrusion. Except for the protrusion gap G , the parameters used in our simulation are kept the same as those prototypes reported in [29,30], so that the fabrication processes should also be the same: $H = 2.14\mu\text{m}$, $L = 1.32\mu\text{m}$, cell gap $d = 4\mu\text{m}$; the ITO tails beside the protrusion are for applying voltage. The black line in Fig. 5(b) shows the simulated VT curve using the experimental protrusion gap $G = 2.68\mu\text{m}$. The peak transmittance is $\sim 82\%$ at 22V. To lower V_p to 15V, we reduce the protrusion gap to $G = 1.5\mu\text{m}$, which is still comparable to the dimension of protrusion width $L = 1.32\mu\text{m}$. As the red line shows in Fig. 5(b), we can achieve 74% transmittance at 15V. Thus, PSBP-08 is a promising candidate for practical applications.

For display applications, gamma shift is another important parameter. The well-known example is multi-domain vertical alignment for LCD TVs. In order to suppress gamma shift, 12 domains are often employed. As a result, the transmittance is greatly reduced because the domain walls block the light.

Here, we investigate the gamma shift of BP LCDs. It has been reported that a single-domain BPLC exhibits greyscale inversion, and to suppress grayscale inversion and widen viewing angle, two-domain structure and biaxial compensation film are needed [32]. We calculated the gray level (GL, G0-G255) from transmittance (T) by $T = (GL/255)^{2.2}$. The gamma curves along the most severe gamma shift direction ($\varphi = 230^\circ$) are plotted in Fig. 5(c). We find the off-axis image distortion index $D(\theta, \varphi) = 0.135$. From previous studies [33,34], as long as $D < 0.2$ the gamma shift is unnoticeable to the human eye. Therefore, for BP LCDs we only need two domains to achieve wide-view and distortion-free off-axis images. By merely using two domains, the effective transmittance should remain high. Moreover, since we are using IPS structure, which is insensitive to the cell gap, the BP LCD should work well for touch panels.

4. Conclusion

Our new PSBP-08 exhibits following outstanding features: 1) its submillisecond response time enables FSC operation, which in turn triples the resolution density and optical efficiency. 2) Its VHR is adequate to support FSC operation. 3) Its blue phase temperature range (from -20°C to 75°C) is adequate for indoor applications. 4) Its average dielectric constant is 87, which is still below the upper limit for bootstrapping driving. Thus, it can be operated at 240 Hz, provided that the high mobility oxide TFTs are employed. 5) Using the triangular electrode structure, PSBP-08 can achieve 74% transmittance at 15V, which enables single-TFT driving. 6) With two-domain structure, our BP LCD offers indistinguishable gamma shift and wide viewing angle. A linear relationship between charging time and ϵ' is proposed and validated by experiment.

Funding

a.u. Vista.

Acknowledgements

The UCF group would like to thank Yishi Weng and Fangwang Gou for technical support and helpful discussions, and JNC for providing the blue phase samples.